ASEAN
Journal of Scientific and Technological Reports
Online ISSN:2773-8752

Research article

Enhanced Electrical and Optical Properties of Cu-Doped ZnO Nanorods Synthesized via Co-Precipitation Method

Onanong Detchaiyaphum[1], **and Buppachat Toboonsung**[1, 2*]

[1] Graduate School, Nakhon Ratchasima Rajabhat University, Nakhon Ratchasima, 30000, Thailand
[2] Faculty of Science and Technology, Nakhon Ratchasima Rajabhat University, Nakhon Ratchasima, 30000, Thailand
* Correspondence: buppachat.t@nrru.ac.th

Citation:
Detchaiyaphum, O.; Toboonsung, B. Enhanced electrical and optical properties of Cu-doped ZnO nanorods synthesized via co-precipitation method. *ASEAN J. Sci. Tech. Report.* **2025**, *28*(5), e259802. https://doi.org/10.55164/ajstr.v28i5.259802.

Article history:
Received: June 14, 2025
Revised: September 9, 2025
Accepted: September 11, 2025
Available online: September 14, 2025

Abstract: Copper-doped zinc oxide (CZO) nanomaterials were prepared by the co-precipitation method, with a 0.5 M $ZnCl_2$ solution as the starting material, doped with 0-5 wt.% $CuCl_2$. The 100 wt.% Cu sample, synthesized without Zn, acts as a pure CuO reference. A 1 M NaOH solution was used as the precipitating agent to adjust the pH to 10. The final product was calcined at 500 °C for 3 h. Morphological analysis using SEM revealed that the CZO samples with 0-5 wt.% Cu exhibited a rod-shaped morphology, whereas the 100 wt.% Cu sample displayed a sheet-like structure with mixed nanoparticles. XRD confirmed the hexagonal wurtzite crystal structure in CZO with no detectable secondary phases, indicating successful incorporation of Cu^{2+} ions into the ZnO lattice. Elemental composition analysis using EDS supported this finding, showing a progressive increase in Cu content from 0.83 wt.% at 1 wt.% doping to 6.03 wt.% at 5 wt.%, accompanied by a corresponding decrease in Zn content. These results suggest that Cu^{2+} ions were effectively substituted for Zn^{2+} within the crystal lattice without forming impurity phases. Optical properties and energy band gap analysis, conducted using fluorescence and ultraviolet-visible spectrophotometry, indicated optimal conditions at 1 wt.% Cu doping. This level corresponded to the lowest band gap energy and the highest electrical conductivity value of 2.71×10^{-3} $(\Omega\cdot cm)^{-1}$, demonstrating a strong correlation between optical absorption and electrical performance. This study presents a systematic investigation into the effect of low-level Cu doping on the structural, optical, and electrical properties of ZnO nanomaterials.

Keywords: Copper-doping; Zinc oxide; Fluorescence spectroscopy; Optical properties; Electrical conductivity

1. Introduction

Nanotechnology currently plays a significant role in advancements across various fields, including medicine, food, cosmetics, electronics, and electrical applications. These developments often enhance the properties of materials, such as electrical and optical performance, to achieve greater efficiency. The synthesis of nanomaterials can be carried out in both thin-film and powder forms, utilizing methods such as spark discharge [1-2], sputtering [3], spray pyrolysis [4], sol-gel processing [5], co-precipitation [6], chemical vapor deposition (CVD) [7], and hydrothermal synthesis [8], among others. Various types of nanomaterials have garnered significant attention, such as titanium dioxide [2], zinc oxide, iron oxide [9], nickel oxide [6], and copper oxide [1], among others. Among these, ZnO is widely studied due to its exceptional optical and electrical properties. As a wide-bandgap semiconductor (3.37 eV), ZnO finds applications in diverse fields, including optoelectronic devices [10], solar cells [11-12], gas sensors [13-14], and antibacterial treatments [15, 16]. Doping with different metals can further enhance ZnO's electrical and optical properties. For instance, doping ZnO with copper (Cu) has been shown to reduce the band gap energy and improve electrical conductivity. Previous studies have indicated that Cu doping reduces the size of nanoparticles and enhances charge carrier mobility, thereby contributing to improved conductivity [17]. However, excessive Cu content may lead to the formation of secondary phases or localized defects, which can hinder electron transport and degrade material performance. Research on Co-doped ZnO nanoparticles prepared via co-precipitation revealed that ZnO retains its hexagonal wurtzite structure even after doping. Doping with 3%, 5%, and 7% Co was found to reduce particle size, while also decreasing the band gap energy, thereby improving electrical conductivity [18]. Similarly, studies on ZnO/CuO composites have demonstrated that increasing CuO concentration progressively reduces grain size, leading to changes in surface morphology and roughness [19]. These findings highlight the importance of precise control over the doping levels to optimize material properties.

While several studies in the literature have described Cu-doped ZnO nanostructures, with an emphasis on optical or structural properties, a comprehensive study of the relationship between low Cu dopant levels, morphology, and electrical properties as a function of the synthetic conditions has not been explored. Focusing on the correlative doping capability of morphology and electrical performance, a detailed investigation of the co-precipitated Cu-doped ZnO (CZO) NRs is presented in this work. The novelty of this work is the systematic analysis of low Cu doping concentrations (0-5 wt.%) under controlled conditions, and a 100 wt.% Cu sample as the CuO pure reference. The 100 wt. % Cu sample, prepared in the absence of the zinc precursor, acts as a pure CuO reference for comparison. Additionally, the ability to produce well-shaped nanorods without the use of surfactants presents a facile and potentially scalable synthetic method. The strong correspondence between the narrowed band gap and enhanced conductivity makes these CZO nanorods promising for optoelectronic devices, such as photodetectors, solar cells, and transparent conducting oxides. Morphological analysis was performed using scanning electron microscopy (SEM), and crystal structure was examined through X-ray diffraction (XRD). Additionally, the optical properties and energy band gap were analyzed using fluorescence spectrophotometry and ultraviolet-visible (UV-Vis) spectrophotometry, respectively. The electrical conductivity of the samples was evaluated using a two-point probe resistance measurement to assess the potential of CZO nanoparticles for electrical applications.

2. Materials and Methods

2.1 Synthesis Process

The copper-doped zinc oxide (CZO) nanomaterials were synthesized using zinc chloride ($ZnCl_2$, Ajax Finechem) as the precursor, with a solution concentration of 0.5 M. Copper chloride ($CuCl_2$, Ajax Finechem) was used as the dopant at concentrations of 0, 1, 3, and 5 wt.% relative to zinc chloride. Additionally, a separate control sample was prepared using only $CuCl_2$ (without $ZnCl_2$) and is referred to as 100 wt.% Cu to denote the absence of Zn precursor. This sample was intended to represent pure CuO for comparative analysis, rather than a doped ZnO system. A 1 M sodium hydroxide (NaOH, Labscan) solution was prepared as the precipitating agent for the co-precipitation process. The $ZnCl_2$ and $CuCl_2$ solutions were prepared using a magnetic stirrer for 15 minutes at 350 revolutions per minute (rpm). Subsequently, the NaOH solution was added dropwise to the mixture while continuously monitoring the pH until it reached 10. The resulting suspension was further stirred for an additional 45 minutes to ensure homogeneity. After stirring, the mixture was left to settle, allowing the precipitate to form. The residue was then washed repeatedly with deionized water until the pH became neutral. The washed precipitate was calcined in a furnace at a heating rate of 5°C/min from room temperature to 500°C, followed by isothermal treatment at 500°C for 3 hours. After calcination, the resulting material was ground into a fine powder using an agate mortar for further characterization.

2.2 Characterization studies

Morphological analysis of the CZO nanomaterials was performed using scanning electron microscopy (SEM, JEOL JSM-6010), which reveals the shape and size of the synthesized particles. Crystal structure analysis was conducted using X-ray diffraction (XRD, Rigaku SmartLab, 40 kV), which enables examination of the crystalline structure. The average crystallite size (D) was calculated using the Scherrer equation (1):

$$D = 0.9\lambda / \beta\cos\theta \tag{1}$$

where β is the full width at half maximum (FWHM) of the XRD peak (in radians), θ is the diffraction angle (in radians), and λ is the wavelength of the Cu-Kα (1.54 Å).

The optical properties were analyzed using fluorescence spectroscopy (Jasco, FP–8300), which measures the luminescence of the samples. This data was further used to calculate the band gap energy using Planck's equation, as shown in Equation 2. For light absorption testing, a UV-Vis spectrophotometer (Thermo Fisher, Genesys 10S) was utilized. The results were analyzed to determine the band gap energy using the Tauc relation. The band gap energy (Eg) [20] was calculated using Equation 3.

$$Eg = hc / \lambda \tag{2}$$

$$(\alpha h\upsilon)^2 = A(h\upsilon - Eg) \tag{3}$$

where Eg is the energy band gap (in eV), h is the Planck constant (6.626×10^{-34} J/s), υ is the frequency (Hz), c is the light velocity (3×10^8 m/s), λ is the wavelength (nm), A is the energy constant, and α is the absorbance coefficient.

The electrical conductivity analysis was conducted by measuring the electrical resistance of the synthesized material using a two-point probe method [21]. A multimeter was connected to two copper electrode plates, with a 100-micrometre-thick plastic sheet placed between them. The sample chamber had a dimension of 10×10 mm^2 [21,22]. A 50-milligram sample of the synthesized material was weighed and placed on the plastic sheet in the chamber on the first copper plate. The second copper plate was then placed on top, and the setup was pressed with a hydraulic press at 500 psi. The measured electrical resistance (UNI-T, UT139) was used to calculate the electrical resistivity of the material using Equation 4. Subsequently, the electrical conductivity was determined using Equation 5 [21, 22]. Each measurement was repeated five times to ensure accuracy.

$$\rho = RA / L \tag{4}$$

$$\sigma = 1 / \rho \tag{5}$$

where ρ is the electrical resistivity ($\Omega \cdot$m), R is the resistance (Ω), A is the surface area (1×1 cm^2), L is the thickness (1 μm), and σ is the electrical conductivity (($\Omega \cdot$m)$^{-1}$), as shown in Figure 1.

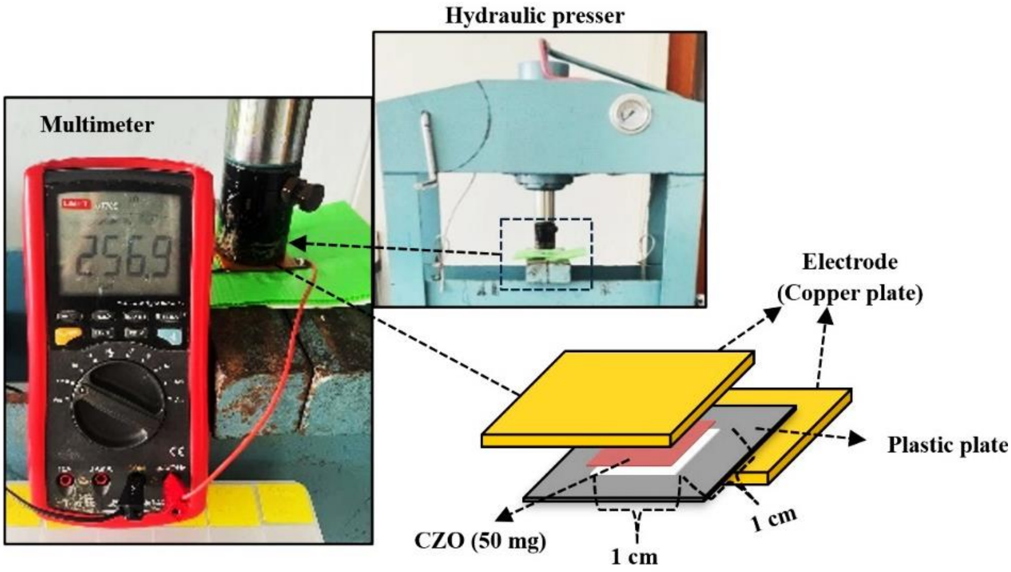

Figure 1. Schematic diagram and experimental setup for measuring the electrical resistance of copper-doped ZnO (CZO) powder.

3. Results and Discussion

3.1 Morphology Analysis

The morphological analysis using scanning electron microscopy (SEM) revealed that the CZO samples with 0-5 wt.% Cu exhibited a nanorod-like structure with irregular sizes, as illustrated in Figure 2. It was considered that the formation of a rod-like structure in the CZO samples may be due to the anisotropic growth inherent in the hexagonal wurtzite structure of the ZnO. In this crystal system, the [001] direction (c-axis) has faster growth kinetics owing to the greater surface energy of the polar (001) plane than the non-polar {100} facets, resulting in the one-dimensional elongation and formation of nanorods [24, 26]. Such growth will be even more favored under the current synthesis conditions: a high pH environment (pH 10), produced by NaOH, not only allows for fast nucleation but also stabilizes the (001) polar surface, leading to preferential c-axis growth. In this study, the co-precipitation method used in the experiment, which is combined with the heat treatment at 500 °C, can afford ample thermal energy for Ostwald ripening (i.e., smaller particles dissolve and redeposit onto larger ones), which is accompanied by the increase of the crystallinity of the nanoparticles and the preferential growth. The lack of organic surfactants or complexing reagents suggests that the morphology is predominantly controlled by the thermodynamic stability of crystal faces in an alkaline medium, rather than by capping action. In comparison to reports by various researchers who observed spherical to irregular-shaped ZnOnanoparticles using the sol-gel route [5], hydrothermal synthesis at lower temperatures [8], and capped agents that limited anisotropic growth. For example, Sangeetha et al. prepared spherical ZnO nanoparticles via the sol-gel method due to the isotropic growth of these particles in alcoholic media [5]. At the same time, Al-Khezraji et al. detected patchy clusters from ZnO/CuO composites studied by precipitation without in situ pH control [19]. The contributions presented in this work provide new insights into the key role of synthesis parameters such as pH and thermal treatment on the final particle shape. The diameters of the nanorods ranged from approximately 290 to 450 nm, while their lengths varied between 1200 and 1520 nm. The aspect ratio (length-to-diameter ratio) was calculated as 4.11, 4.14, 3.66, and 2.87 for doping levels of 0%, 1%, 3%, and 5% wt.%, respectively. The highest aspect ratio was observed at 1 wt.% Cu doping. In contrast, the sample containing 100 wt.% Cu showed a sheet-like structure with mixed nanoparticles. This sample was synthesized without any $ZnCl_2$, and thus, in the absence of Zn^{2+} ions, copper ions (Cu^{2+}) precipitate as $Cu(OH)_2$ under alkaline conditions, which readily decomposes to monoclinic CuO upon calcination at 500 °C. This explains the distinct sheet-like morphology and phase formation, consistent with the XRD and EDS results. This suggests that the presence of excess Cu results in a distinct growth mechanism and morphology. Despite variations in copper content, the overall rod-shaped morphology was preserved in the doped samples, suggesting that low-level Cu doping does not significantly alter the structural evolution of ZnO during synthesis.

3.2 Crystal Structure Analysis

X-ray diffraction (XRD) patterns confirmed that CZO samples with 0-5 wt.% Cu exhibited the hexagonal wurtzite structure of ZnO, consistent with JCPDS standard card number 36-1451 (Figure 3). The diffraction peaks corresponding to the (100), (002), (101), (102), (110), (103), (200), (112), and (201) planes were observed, indicating good crystallinity. For the 100 wt.% Cu sample, the diffraction pattern matched the monoclinic structure of CuO (JCPDS No. 48-1548), with characteristic peaks at (110), (11-1), (111), (200), (20-2), (020), (202), (11-3), (113), and (220). No additional peaks related to metallic Cu or secondary phases were detected in the CZO samples with low Cu concentrations. The absence of detectable Cu-related peaks suggests that Cu^{2+} ions have successfully substituted for Zn2+ ions within the ZnO lattice without forming secondary phases, which is consistent with previous studies [12, 17]. Using the Scherrer equation, the average crystallite size was estimated to be approximately 25 nm for CZO samples with 0-5 wt.% Cu, whereas the 100 wt.% Cu sample had a smaller crystallite size of about 16 nm. It should be noted that the 100 wt.% Cu sample was synthesized in the absence of any zinc precursor. As a result, the formation of a monoclinic CuO phase is expected, since Cu^{2+} ions first hydrolyze to $Cu(OH)_2$, which subsequently decomposes into CuO during calcination. This phase is structurally and compositionally distinct from the Cu-doped ZnO series, thereby serving as a pure CuO reference sample.

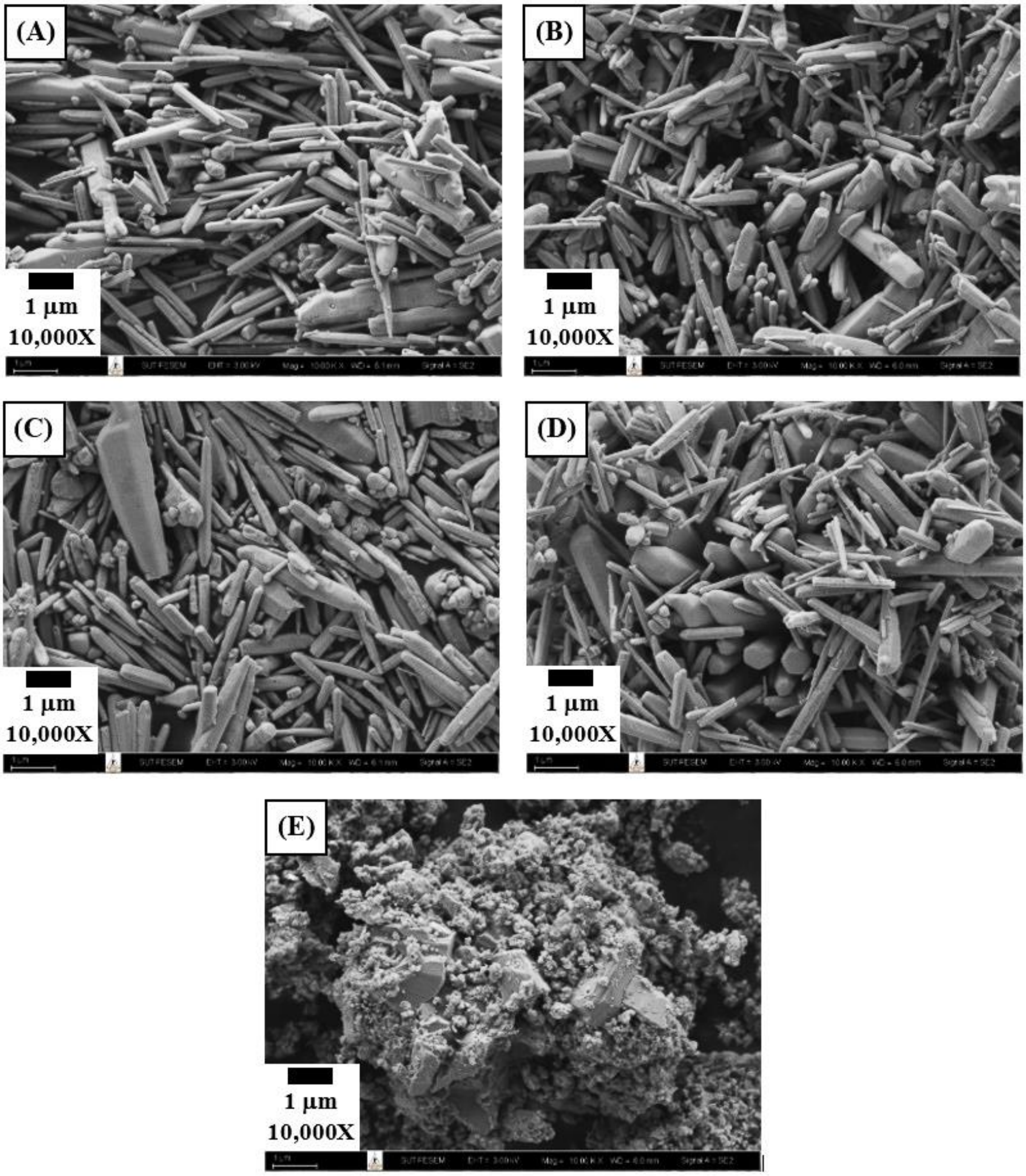

Figure 2. SEM images of CZO for (A) 0 wt.%, (B) 1 wt.%, (C) 3 wt.%, (D) 5 wt.%, and (E) 100 wt.% (control sample).

3.3 EDS Analysis and Elemental Composition

To confirm the successful incorporation of Cu into the ZnO lattice at low doping concentrations (1-5 wt.%), energy-dispersive X-ray spectroscopy (EDS) was conducted to determine the elemental composition of each sample. The results, summarized in Table 1, reveal a progressive increase in Cu content from 0.83 wt.% at 1 wt.% doping to 6.03 wt.% at 5 wt.% doping, accompanied by a corresponding decrease in Zn content. These findings support the hypothesis that Cu^{2+} ions are substitutionally incorporated into the ZnO lattice without forming secondary phases detectable by X-ray diffraction (XRD). In contrast, the 100 wt.% Cu sample exhibits a drastic increase in Cu content (71.81 wt.%) and a sharp decrease in Zn (1.51 wt.%), indicating the formation of a distinct CuO phase. The EDS data provide evidence for the successful incorporation of Cu into the ZnO lattice, with increasing Cu content as the doping level increases, at 1 wt.% Cu doping, the amount of

Cu increased slightly without significantly altering the Zn/O ratio, suggesting a uniform distribution of the dopant within the lattice. However, at higher doping levels (3-5 wt.%), the increase in Cu content corresponded to a decrease in Zn, which is indicative of Cu^{2+} substituting Zn^{2+} ions within the crystal structure, for the 100 wt. The negligible Zn content (1.51 wt.%) in the Cu sample confirms that the material consists predominantly of pure CuO nanostructures. This compositional evidence aligns with the XRD results, which show a monoclinic CuO phase, and the distinct sheet-like morphology observed in the SEM image. These findings strongly support the hypothesis that, at low doping levels (1-5 wt.%), Cu^{2+} ions successfully substitute Zn^{2+} within the ZnO lattice without forming secondary phases.

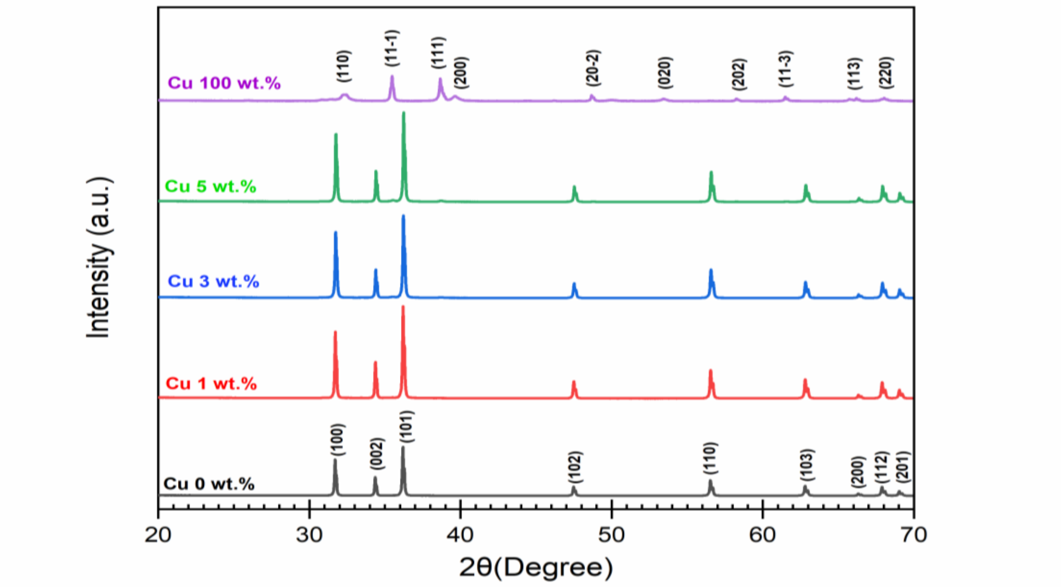

Figure 3. XRD pattern of 0-100 wt.% CZO.

Table 1. Elemental composition of CZO samples obtained from EDS analysis.

Cu doping (wt.%)	Zn (wt.%)	O (wt.%)	Cu (wt.%)
0	72.38	26.85	0.77
1	76.86	22.31	0.83
3	72.97	24.77	2.26
5	71.74	22.23	6.03
100 (control sample)	1.51	26.68	71.81

3.4 Fluorescence Spectroscopy Analysis

The luminescence of the samples was analyzed using fluorescence spectroscopy, and the peaks were modeled under the spectrum data using a Lorentzian function, resulting in three distinct peaks as shown in Figure 4. The CZO samples at concentrations of 0, 1, 3, 5, and 100 wt.% exhibited luminescence in the violet region (323-398 nm), corresponding to electron excitation from the ground state to a higher energy level. This excitation process is designated as Peak 1. Peak 2, observed in the blue region (422-444 nm), corresponds to fluorescence emission as electrons returned to the ground state. Peak 3, located in the green area (548-563 nm), is attributed to defect-related recombination, often associated with oxygen vacancies or zinc interstitials, which produce deep-level emission. These wavelengths were used to calculate the band gap energy using Planck's equation, where the band gap energy for excitation and fluorescence was found to be lower for Cu doping at 1, 3, and 5 wt.% compared to undoped ZnO with values of 3.11 eV and 2.78 eV, respectively. The reduction in band gap energy at 1 wt.% Cu correlates with enhanced charge carrier generation, which contributes to the improvement in electrical conductivity. However, at higher doping levels (3–5 wt.%), the slight increase in band gap energy and the presence of defect-related emission peaks suggest that excess Cu introduces localized states within the band gap, which may act as recombination or scattering centers. Furthermore, EDS analysis provided quantitative evidence of Cu incorporation at 1 wt.% Cu doping, the Zn/O ratio remained relatively unchanged, suggesting uniform distribution of Cu within the lattice; however, at 100 wt.% Cu, Zn content dropped to only 1.51 wt.%, confirming that it corresponded to pure CuO rather than a doped ZnO system. These findings strongly support the conclusion that low-level Cu doping effectively modifies the electronic structure of ZnO, reducing the band gap and enhancing light absorption. In contrast, excessive Cu content introduces localized defect states or impurity phases that act as scattering centers, diminishing carrier mobility and overall performance.

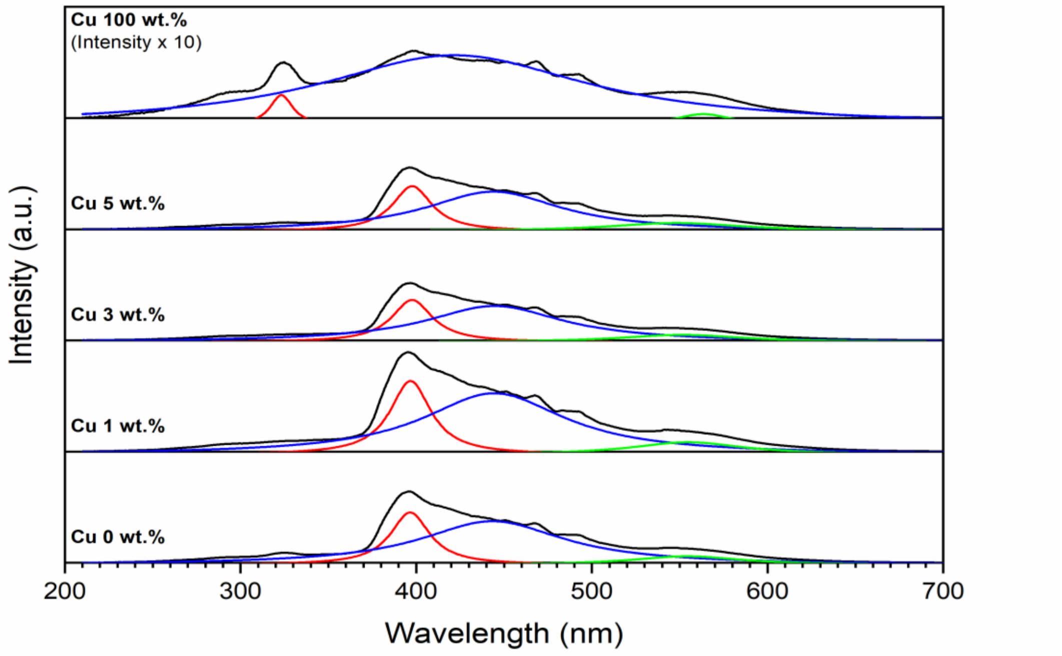

Figure 4. Fluorescence spectra of 0-100 wt.% CZO.

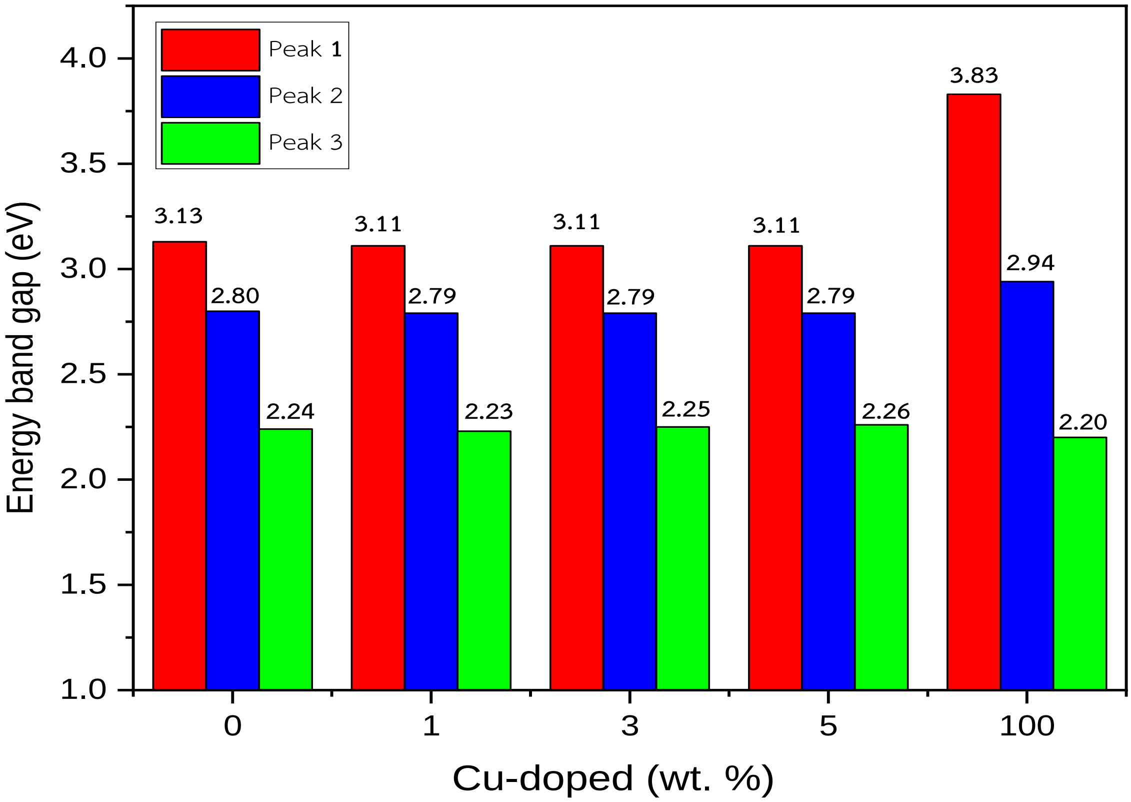

Figure 5. Three peaks of the energy band gap from fluorescence analysis in Figure 4.

3.5 UV-Vis Spectroscopy Analysis

The optical absorption properties of ZnO doped with Cu at concentrations of 0, 1, 3, 5, and 100 wt.% were analyzed using UV-Vis spectroscopy, as shown in Figure 6. The Tauc method was applied to calculate the band gap energy using Equation (3). The absorption occurred in the visible range (violet), with maximum wavelengths at 402, 428, 430, 449, and 350 nm. The corresponding band gap energies were calculated as 2.90, 2.72, 2.82, 2.83, and 2.16 eV, respectively. The lowest band gap energy was observed at 2.72 eV for Cu doping at 1 wt.%. It is noted that the band gap of nanomaterials is not only sensitive to the dopant concentrations, but also to the particle size and morphology. In this work, the diameter of the nanorod was found to decrease with an increase in Cu content, which generally results in a blue shift (an increase in band gap) due to quantum confinement. However, the measured red shift (from 2.90 eV to 2.72 eV) indicates that the effect of Cu doping prevails, primarily due to the hybridization of Cu 3d states with O 2p orbitals at the valence band edge, which narrows the band gap [23]. Such trends are opposite at high doped levels (3-5 wt.%), and the higher band gap of the Cu-doped ZnO might be attributed to the generation of defect states such as oxygen vacancies or the presence of Cu interstitials, which form interstitial levels in the mid-gap and counteract the narrowing effect. This observation contrasts with the study by Sajjad et al. [17], in which the band gap decreased continuously with an increase in copper content. This deviation can be attributed to the differences in doping units (wt.% vs. mol%) and the emergence of defect-related effects at higher doping levels in this study. These results reveal the existence of an optimal doping range for minimizing the band gap. This behavior has been previously reported by Cu-doped ZnO systems, in which the introduction of Cu^{2+} ions produces an impurity level close to the valence band toward the band gap energy [17,23]. The observed decrease in band gap from 2.90 eV (0 wt.%) to 2.72 eV (1 wt.% Cu) supports the successful substitution of Cu^{2+} into the ZnO lattice. The optical absorption analysis, performed using UV-Vis spectroscopy, showed consistent trends with the fluorescence results. CZO samples doped with 1 wt.% Cu exhibited the lowest band gap energy of 2.72 eV, confirming the effectiveness of low-level Cu doping in modifying the electronic structure of ZnO. At higher Cu concentrations (3 and 5 wt.%), the band gap energy increased slightly to 2.82 eV and 2.83 eV, respectively, aligning with the observed increase in defect-related emission from fluorescence measurements. This correlation between fluorescence and UV-Vis spectroscopy supports the hypothesis that Cu^{2+} ions are substitutionally incorporated into the ZnO lattice, leading to a narrowing of the band gap and enhanced optical absorption. In contrast, the sample containing 100 wt.% Cu showed the lowest band gap energy (2.16 eV), which is interpreted as pure CuO rather than a doped system.

3.6 Electrical Conductivity Analysis

The electrical conductivity of the synthesized CZO nanomaterials was evaluated by measuring the electrical resistance and subsequently calculating the resistivity and conductivity using Equations (4) and (5), respectively. The results are summarized in Figure 7 and discussed below. The undoped ZnO sample (0 wt.% Cu) exhibited an electrical conductivity of 2.18×10^{-3} $(\Omega\cdot cm)^{-1}$, upon doping with 1 wt.% Cu, the conductivity increased to 2.71×10^{-3} $(\Omega\cdot cm)^{-1}$, which is the highest value observed in this study. Further increasing the Cu content to 3 wt.% and 5 wt.% resulted in a decrease in conductivity to 1.88×10^{-3} and 0.93×10^{-3} $(\Omega\cdot cm)^{-1}$, respectively. The sample containing 100 wt.% Cu showed a conductivity of 1.78×10^{-3} $(\Omega\cdot cm)^{-1}$, which is lower than that of the 1 wt.% doped sample but higher than that of the undoped ZnO. The reduction in band gap energy at 1 wt.% Cu correlates with enhanced charge carrier generation, leading to improved electrical conductivity. This suggests that Cu^{2+} ions were successfully incorporated into the ZnO lattice, contributing additional free carriers that enhance conductivity. However, further increases in Cu content beyond 1 wt.% led to a decline in electrical conductivity. Excessive Cu content introduces localized defect states that act as recombination centers or scattering sites, reducing carrier mobility and overall conductivity. These defects may arise from the formation of impurity phases or distortions in the crystal lattice due to excess Cu, which hinder the effective movement of charge carriers. Comparing these results with previous studies, Redwanul I. et al. reported an electrical conductivity of 0.0986×10^{-5} $(\Omega\cdot m)^{-1}$ for undoped ZnO nanoparticles [27], while Shahroz S. et al. found a conductivity of 1.09×10^{-4} $(\Omega\cdot cm)^{-1}$ for CuO nanoparticles [28]. However, they also noted a decline in conductivity at higher doping levels due to enhanced carrier scattering. This study confirms that optimal Cu doping at 1 wt.% significantly improves the electrical properties of ZnO nanomaterials, making them promising candidates for optoelectronic applications such as photodetectors and solar cells.

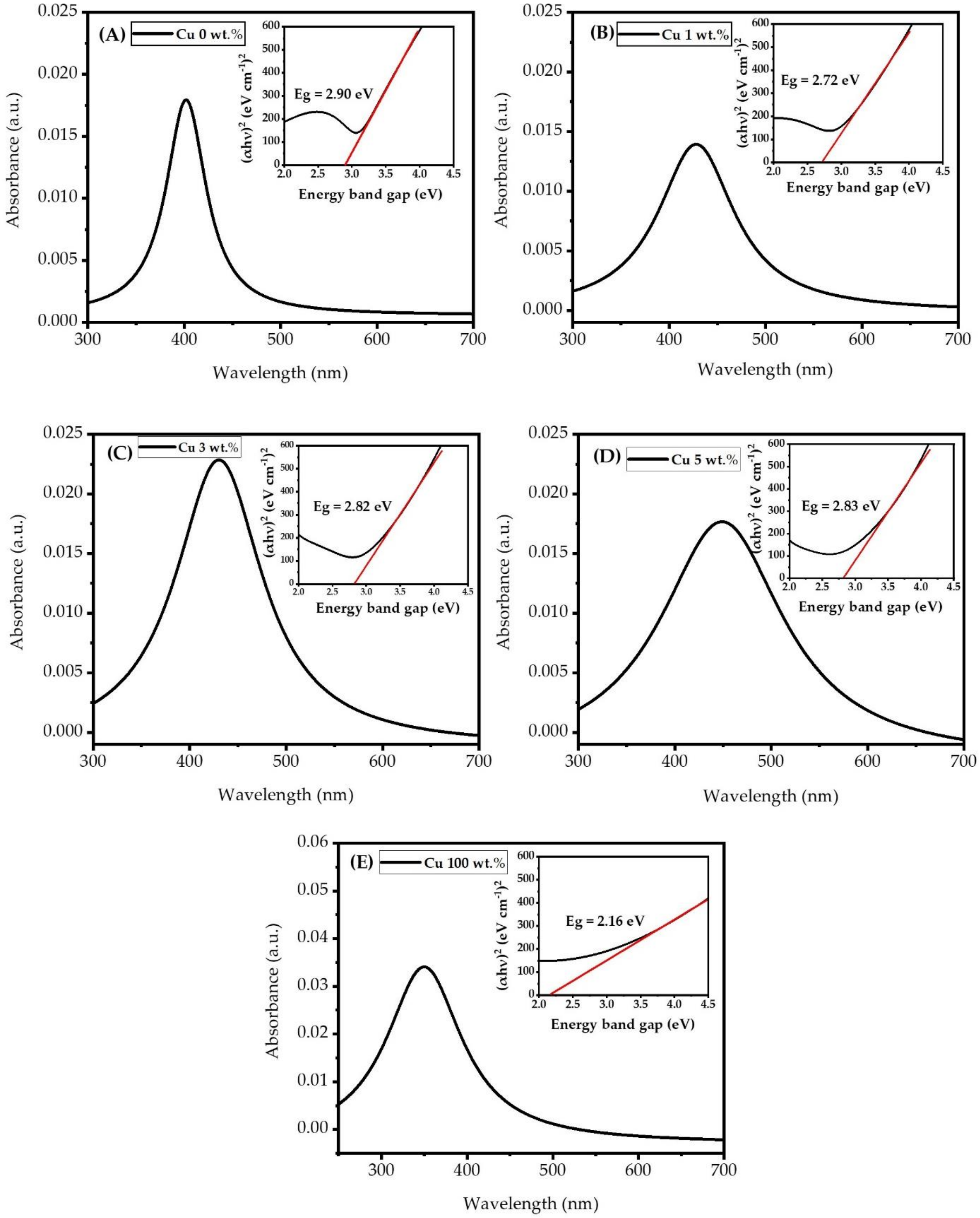

Figure 6. The graph of light absorption and the inset energy band gap from UV-VIS spectroscopy of CZO for (A) 0 wt.%, (B) 1 wt.%, (C) 3 wt.%, (D) 5 wt.%, and (E) 100 wt.%, respectively.

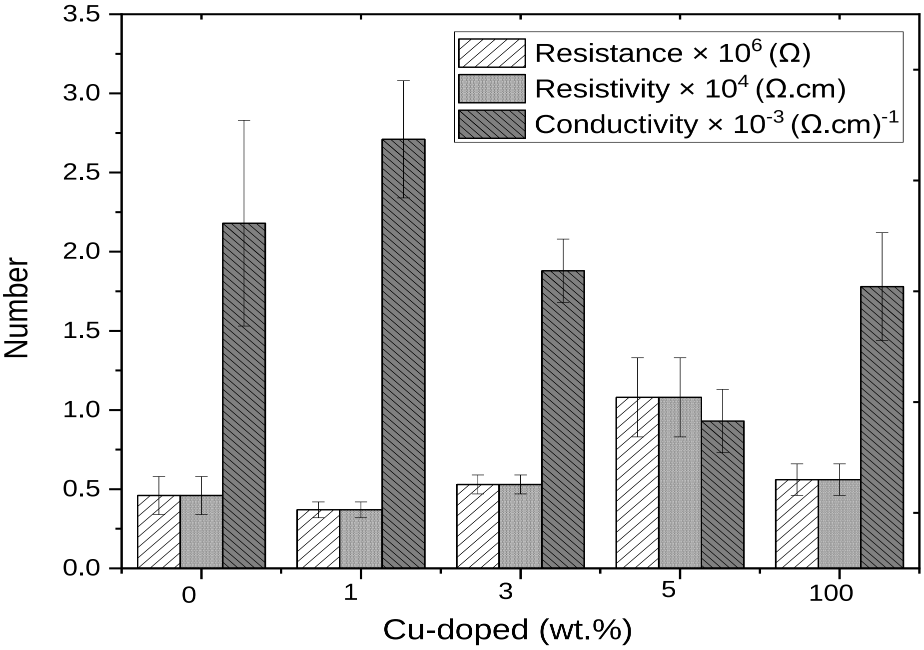

Figure 7. Electrical resistance, electrical resistivity, and electrical conductivity of CZO.

4. Conclusions

Copper-doped zinc oxide (CZO) nanomaterials with doping levels of 0, 1, 3, and 5 wt.% exhibited a nanorod morphology, while the sample containing 100 wt.% Cu displayed an irregular sheet-like structure with mixed nanoparticles. X-ray diffraction (XRD) analysis confirmed that the CZO nanomaterials retained the hexagonal wurtzite crystal structure within the low Cu doping range (0-5 wt.%), with no detectable secondary phases observed. This suggests that Cu^{2+} ions were successfully incorporated into the ZnO lattice without forming separate Cu or CuO phases. The tunable band gap in CZO nanorods arises from a synergistic interplay between Cu doping, particle size, and nanorod morphology, with doping being the primary tuning parameter. The electrical conductivity measurements revealed that the highest value of 2.71×10^{-3} $(\Omega{\cdot}cm)^{-1}$ was achieved at 1 wt.% Cu doping, which also corresponded to the lowest band gap energy based on both fluorescence and UV-Vis absorption analyses. These results indicate a strong correlation between optical and electrical properties in CZO nanomaterials. The reduction in band gap energy at 1 wt.% Cu correlates with enhanced charge carrier generation, leading to improved electrical conductivity. This finding supports the hypothesis that Cu^{2+} ions effectively substitute Zn^{2+} ions, enhancing charge transport efficiency. However, increasing Cu content beyond this optimal level resulted in a decrease in conductivity. Excessive Cu content introduces localized defect states that act as recombination centers or scattering sites, reducing carrier mobility and overall conductivity. This study demonstrates that moderate Cu doping significantly enhances the electrical and optical properties of ZnO nanomaterials. The optimal performance at 1 wt.% Cu highlights the importance of precise control over doping concentration to avoid defect-induced carrier scattering. The systematic investigation conducted in this work reveals that low-level Cu doping at 1 wt.% not only enhances electrical conductivity but also tunes the band gap energy, offering new opportunities for CZO in optoelectronic device engineering.

5. Acknowledgements

This work was supported by Nakhon Ratchasima Rajabhat University, Nakhon Ratchasima, Thailand. We would like to thank Khajondach Viangsong and Napaporn Thaweesaeng for their assistance with the preparation and analysis of UV-VIS spectroscopy and electrical resistance measurements. The XRD measurements and fluorescence spectroscopy were supported by Dr. Panadda Phansamdaeng, with contributions from Samart Tuaykratok and Keardtipong Jadnok..

Author Contributions: In this article, the following fields of work were carried by: Conceptualization, Buppachat Toboonsung.; methodology, Onanong Detchaiyaphum and BT.; validation, OD and BT.; formal analysis, BT. investigation, OD and BT.; resources, OD and BT.; data curation, BT.; writing—original draft preparation, OD.; writing—review and editing, BT.; visualization, OD and BT.; supervision, OD and BT; project administration, OD and BT.; funding acquisition, OD and BT. In addition, all authors have read and agreed to the published version of the manuscript.

Conflicts of Interest: The authors declare that they have no conflicts of interest.

References

[1] Traiwatcharanon, P.; Pon-On, W.; Zacharias, M.; Wongchoosuk, C. Electrochemical copper oxide nanoparticles-based sensor for butachlor plus propanil herbicide detection. *J Mater Sci: Mater Electron.* **2024**, *35*, 651. https://doi.org/10.1007/s10854-024-12419-5.

[2] Toboonsung, B. (2019) Surface morphologies and durability on water contact angle of titanium dioxide nanoparticle thin films. *Key Eng. Mater.* **2019**, *798*, 158-162. https://doi.org/10.4028/www.scientific.net/KEM.798.158.

[3] Nagabharana, R.M.; Kumaraswamy, G.N.; Susheel, K.G.; Umananda, M.B. Effect of thermal annealing on structural and electrical properties of TiO_2 thin films. *Thin Solid Films* **2020**, *710*, 138262. https://doi.org/10.1016/j.tsf.2020.138262.

[4] Cuadra, J.G.; Estrada, A.C.; Oliveira, C.; Abderrahim, L.A.; Porcar, S.; Fraga, D.; Trindade, T.; Seabra, M.P.; Labrincha J.; Carda J.B. Functional properties of transparent ZnO thin films synthesized by using spray pyrolysis for environmental and biomedical applications. *Ceram. Int.* **2023**, *49*, 32779-32788. https://doi.org/10.1016/j.ceramint.2023.07.246.

[5] Sangeetha, A.; Jaya Seeli, S.; Bhuvana, K.P.; Abdul Kader, M.; Nayak, S.K.; Correlation between calcination temperature and optical parameter of zinc oxide (ZnO) nanoparticles. *J. Sol-Gel Sci. Technol.* **2019**, 91, 261-272. https://doi.org/10.1007/s10971-019-05000-8.

[6] Toboonsung, B. Structure, magnetic property and energy band gap of Fe-doped NiO nanoparticles prepared by co-precipitation method. *Key Eng. Mater.* **2017**, *751*, 379-383. https://doi.org/10.4028/www.scientific.net/KEM.751.379

[7] Narin, P.; Kutlu-Narin, E.; Lisesivdin, S.B.; Growth dynamics of mist-CVD grown ZnO nanoplatelets. *Physica B: Condens. Matter.* **2021**, *614*, 413028. https://doi.org/10.1016/j.physb.2021.413028.

[8] Yaowen, H.; Junhui, Y.; Yun, W.; Jiayao, J.; Jialu, W.; Haiyan, T.; Ying, Y.; Tianqi, W.; Lin, X.; Dong X. Femtosecond laser combined with hydrothermal method to construct three-dimensional spatially distributed wurtzite ZnO micro/nanostructures to enhance photocatalytic properties. *Langmuir*, **2024**, *40*, 3892-3899. https://doi.org/10.1021/acs.langmuir.3c03840.

[9] Kumar, M.; Dede Heri, Y.Y.; Mani, G.; Bogeshwaran, K.; Fatmah, A.A.; Reem, A.H. Biological synthesis and characterization of iron oxide (FeO) nanoparticles using *Pleurotus citrinopileatus* extract and its biomedical applications. *Biomass Convers. Biorefin.* **2024**, *14*,12575-12585. https://doi.org/10.1007/s13399-023-04382-8.

[10] Ahmed Adel, A.A.; Hadia, N.M.A.; Meshal, A.; Mohamed, S.; Abdel-Hamid, I.M.; Fernández, S.; Rabia, M. Development of CuO nanoporous material as a highly efficient optoelectronic device. *Appl. Phys. A* **2022**, *128*, 321. https://doi.org/10.1007/s00339-022-05447-7.

[11] Sahar, I.S.; Maryam, A.A.; Wedian, K.A.; Ahmed, N.A. Low-cost applications by simple chemical method: solar cell and photodetector. *Int. J. Nanosci.* **2024**, *23(2)*, 2350063. https://doi.org/10.1142/S0219581X23500631.

[12] Aneesiya, K.R.; Cindrella, L. Localized surface plasmon resonance of Cu-doped ZnO nanostructures and the material's integration in dye sensitized solar cells (DSSCs) enabling high open-circuit potentials. *J Alloys Compd.* **2020**, *829*, 154497. https://doi.org/10.1016/j.jallcom.2020.154497

[13] Junfeng, C.; Haijun, Y.; Ke, Z.; Ying, Z.; Deshuo, M.; Yeguo, S. Integration of ZnO and Au/ZnO nanostructures into gas sensor devices for sensitive ethanolamine detection. *ACS Appl Nano Mater.* **2023**, *6(7)*, 5994-6001. https://doi.org/10.1021/acsanm.3c00350

[14] To Thi, N.; Dang, T.T.L.; Nguyen, V.D.; Chu, T.X.; Sven, I.; Xuan, T.V.; Nguyen D.H. A sigh-performance hydrogen gas sensor based on Ag/Pd nanoparticle-functionalized ZnO nanoplates. *RSC Advances* **2023**, *13*, 13017-13029. https://doi.org/10.1039/D3RA01436C.

[15] Thambidurai, S.; Gowthaman, P.; Venkatachalam, M.; Suresh, S. Enhanced bactericidal performance of nickel oxide-zinc oxide nanocomposites synthesized by facile chemical co-precipitation method. *J Alloys Compd.* **2020**, *830*, 154642. https://doi.org/10.1016/j.jallcom.2020.154642.

[16] Negi, P.B.; Rana, A.; Joshi, N.C.; Mishra, A.; Manoj, C.L.; Sunori, S.K. Synthesis, characterization and antimicrobial activity of zinc oxide nanoparticles against *Escherichia coli* and *Salmonella enterica*-water borne pathogens. *Asia Pac J Sci Technol.* **2024**; *29(03)*, APST-29. https://doi.org/10.14456/apst.2024.40.

[17] Sajjad, M.; Ullah, I.; Khanb, M.I.; Khanc, J.; Khana, M.Y.; Qureshi, M.T. Structural and optical properties of pure and copper doped zinc oxide nanoparticles. *Results Phys.* **2018**, *9*, 1301-1309. https://doi.org/10.1016/j.rinp.2018.04.010

[18] Ravichandran, A.T.; Karthick, R. Enhanced photoluminescence, structural, morphological and antimicrobial efficacy of Co-doped ZnO nanoparticles prepared by Co-precipitation method. *Results Mater.* **2020**, *5*, 100072. https://doi.org/10.1016/j.rinma.2020.100072.

[19] Al-Khezraji, A.A.R.; Abd Ali, H.R.; Yousif, A.A.; Abed, H.R. Effect of mixed ZnO/CuO nanoparticles on the structural, morphological, and topographical properties. *J Phys Conf Ser.* **2021**, *1963(1)*, 012053. https://doi.org/10.1088/1742-6596/1963/1/012053.

[20] Meryem, L.Z.; Touidjen, N.E.H.; Aida, M.S.; Aouabdia, N.; Rouabah, S. Growth of undoped ZnO thin films by spray pyrolysis: effect of precursor concentration. *J Opt.* **2023**, *52*, 1782-1788. https://doi.org/10.1007/s12596-022-01079-5.

[21] Montes, J.M.; Cuevas, F.G.; Cintas, J. Electrical resistivity of metal powder aggregates. *Metall Mater Trans B.* **2007**, *38*, 957-964. https://doi.org/10.1007/s11663-007-9097-3.

[22] Kingpho, P.; Toboonsung, B. Improvement of the Electrical properties of ZnO nanomaterials with Fe by Co-precipitation method. *Curr Appl Sci Technol.* **2025**, *25(3)*, e0263485. https://doi.org/10.55003/cast.2024.263485.

[23] Dejam, L.; Kulesza, S.; Sabbaghzadeh. J.; Ghaderi, A.; Solaymani, S.; Talu. S.; Bramowicz, M.; Amouamouha, M.; Salehi shayegan, A.H.; Sari, A.H. ZnO, Cu-doped ZnO, Al-doped ZnO and Cu-Al doped ZnO thin films: Advanced micro-morphology, crystalline structures and optical properties. *Results Phys.* **2023**, *44*, 106209. https://doi.org/10.1016/j.rinp.2023.106209.

[24] Lin, J.H.; Patil R.A.; Devan, R.S.; Liu, Z.A.; Wang, Y.P.; Ho, C.H.; Liou, Y.; Ma Y.R. Photoluminescence mechanisms of metallic Zn nanospheres, semiconducting ZnO nanoballoons, and metal-semiconductor Zn/ZnO nanospheres. *Sci Rep.* **2014**, *4*, 6967. https://doi.org/10.1038/srep06967.

[25] Mahroug, A.; Mari, B.; Mollar, M.; Boudjadar, I.; Guerbous, L.; Henni, A.; Selmi N. Studies on structural, surface morphological, optical, luminescence and UV photodetection properties of sol-gel Mg doped ZnO thin films. *Surf Rev Lett.* **2018**, *26(03)*, 1850167. https://doi.org/10.1142/S0218625X18501676.

[26] Gaur, L.K.; Gairola, P.; Gairola, S.P.; Mathpal, M.C.; Kumar, P.; Kumar, S.; Kushavah, D.; Agrahari, V.; Aragon, F.F.H.; Maria, A.G.S.; Swart, H.C. Cobalt doping induced shape transformation and its effect on luminescence in zinc oxide rod-like nanostructures. *J Alloys Compd.* **2021**, *868*, 159189. https://doi.org/10.1016/j.jallcom.2021.159189.

[27] Redwanul I, Suprio SS, Reana R, Nayeemul I, Torikul I. Unveiling the synthesis, characteristics, electrical conductivity, photocatalytic activity, and electrochemical activity of eco-friendly zinc oxide nanoparticles. *Adv. Sens. Energy Mater.* **2024**, *3*, 100105. https://doi.org/10.1016/j.asems.2024.100105.

[28] Shahroz, S.; Awais, K.; Zaid, M.A.; Thamer, A.; Arshad, A.; Abdul, J.; Yasmin Begum M.; Kandasamy G. A comparative analysis of optical and electrical properties of pure CuO and Zn doped CuO nanoparticles for optoelectronic device applications. *J Sol-Gel Sci Technol.* **2025**, *113*, 213-224. https://doi.org/10.1007/s10971-024-06591-7